Image Simulation for GF-5 Visual and Infrared Multispectral Sensor

Zhang Wenjuan(1), Shi Mengmeng(2), Zhang Bing(1)(3), Li Yunduan(4), Dai Haishan(4)

[1]Key Laboratory of Digital Earth Science, Institute of Remote Sensing and Digital Earth, Chinese Academy of Sciences, Beijing 100094, China;
[2]Xi'an University of Science and Technology, Xi'an, 710054,China
[3]University of Chinese Academy of Sciences, Beijing 100049, China
[4]Shanghai Institute of Satellite Engineering, Shanghai, 200240, China
Email: zhangwj@aircas.ac.cn; shimeng123_happy@163.com; zhangbing@aircas.ac.c.cn; liyunduan1976@126.com; dhs1314@126.com

KEY WORDS: GF-5, Visual and Infrared Multispectral Sensor (VIMS), Image Simulation, Spectral Correlation Analysis

ABSTRACT: Modeling the image system is a critical component in understanding data characteristics, producing sample products, exploring potential applications and predicting mission utility. The Visual and Infrared Multispectral Sensor (VIMS) equipped on the Gaofen-5 (GF-5) satellite is certainly one of the most outstanding systems that delivers a large number of the Earth's surface data in the 0.4–12.5 μm spectral range with 12 broad bands since launch. Before its launch, an image simulation method is proposed base on the adjacent channels of existing sensors. ASTER data is chosen as the simulation source based on the analysis of sensor characteristics. There are many types of objects are selected from the JHU spectral library to analyze the spectral correlation between VIMS and ASTER bands. The channel conversion model is established to simulated VIMS image data through Partial Least Squares Regression and evaluated by 10-fold-cross-validation, and a test case in the Daya Bay area is given. The error analysis shows that the mean relative error is 2.551% and the value is less than 1% in most cases.

1. INTRODUCTION

The Gaofen-5 (GF-5) satellite is the fifth satellite of China High-resolution Earth Observation System project. It was developed by the China Aerospace Science and Technology Corporation (CASC) and launched on 9 May 2018. The satellite, which is China's first high-resolution satellite for atmospheric observation, is also the first hyperspectral imaging satellite developed by China. The main objective of the satellite is to effectively monitor the atmospheric environment, water environment and ecological environment (Yunzhu Sun et al., 2017).n the satellite. It has some features: wide spectral range (0.45μm-12.5μm), multiple spectral bands (12 bands), high spatial resolution (20m(VNIR-SWIR)/ 40m(MWIR,TIR), and high accuracy of radiation calibration (visible short wavelength 5% / medium and long wavelength 1K), etc. (Zhao Yanhua et al, 2017).Image simulation constructs the process of data acquisition via mathematical models, and simulates the remote sensing images (Borner et al., 2001). The simulation not only provides an important basis of the analysis and optimization of optical payload parameters designs, but also helps researchers to understand the payload imaging process and its influencing factors. It provides data to support payload application and the algorithm research (Liu et al., 2015).It has become an important part in the development of new remote sensors (Zhang Wenjuan, 2008; Parente et al., 2010; Segl et al., 2015). Based on the spectral correlation of the adjacent channels and the ASTER data, this paper proposes an image simulation method to simulate the VIMS data before launched.

2. DATA and METHODOLOGY

The remote sensing image of adjacent channels is considered to have a strong correlation. This theory has been successfully applied to many fields, such as multi-spectral and hyperspectral data information extraction, parametric inversion, etc. Based on spectral and spatial correlation, a method to evaluate the signal-to-noise ratio of hyperspectral data was presented by Gao et al. (2008), and a multi-spectral data compression model was proposed by Magli (2009). Tang et al. (2015) retrieved thermal infrared emissivities based on this mechanism. It shows that there is a strong correlation between adjacent channels regardless of the wavelength position.

The VIMS simultaneously acquire the data of the visible and near-infrared, short wave infrared, middle wave infrared, and thermal infrared bands, Spectral and spatial features are shown in Table 1. It can be seen that image simulation can be performed based on the correlation with adjacent channels of other remote sensing data. The workflow in this paper is designed as follows: characterizes of the VIMS is analyzed to select the simulation source and acquire the typical spectral data. The spectral data of the VIMS channel and its corresponding source channel is calculated based on spectral response functions. Data correlation between the VIMS channel and its corresponding source channel is analyzed. The method is constructed and the accuracy analysis is implemented.

Table 1. Spectral and spatial features of VIMS of GF-5, and of ASTER.

	VIMS	**ASTER**
Spectral range (μm) and Spectral Sample	VNIR: band1: 0.45–0.52;	VNIR: band1: 0.52–0.6;

Interval (SSI)	band2: 0.52–0.6; band3: 0.62–0.68; band4: 0.76–0.86 SWIR: band5: 1.55–1.75; band6: 2.08–2.35 MIR: band7: 3.5–3.9; band8: 4.85–5.05 TIR: band9: 8.01–8.39; band10: 8.42–8.83; band11: 10.3–11.3; band12: 11.4–12.5	band2: 0.63–0.69; band3: 0.78–0.86 SWIR: band4: 1.6–1.7; band5: 2.145–2.185; band6: 2.185–2.225; band7: 2.235–2.285; band8: 2.295–2.365; band9: 2.36–2.43 TIR: band10: 8.125–8.475; band11: 8.475–8.825; band12: 8.925–9.275; band13: 10.25–10.95; band14: 10.95–11.65
Spatial resolution	VNIR/SWIR: 20 m MIR/TIR: 40 m	VNIR: 15 m SWIR: 30 m TIR: 90 m
Swath width	60 km	60 km

2.1 Source sensor

In general, the closer the source channel is to the simulated band, the higher correlation between spectral radiation data (Gao et al., 2008). Therefore, it is preferred to select the optical payloads whose band setting is similar to that of the GF-5 VIMS. According to the band setting of the VIMS shown in Table 1, ASTER is selected as the source sensor. Even though the middle wave infrared channels are lacked in the ASTER data, it is rich in the visible near-infrared, short- wave infrared and thermal infrared channel bands. Moreover, it has the most similar channel setting compared to the VIMS. Therefore, the ASTER data is selected as the source data for simulation, while the middle wave infrared part can be simulated by short wave infrared and thermal infrared bands.

2.2 Spectral Data

Based on the composition of typical spectral libraries, the spectral data of many types of object were selected corresponding to the spectral characterizes of the VIMS and the ASTER sensor. The spectral range of data is from 0.45μm to 12.5μm.The number of these data is 60 and they are all from the JHU spectral library, which including man-made materials, water, soil and 3 other typical categories (Baldridge, 2009). The spectral sample interval and range are all uniformed in this paper. The spectral sample interval is 1 nm and the range is from 0.42 to 12.5μm. These 60 spectral data include 19 types of man-made materials (including asphalt, concrete, paint, metal, brick, etc.), 2 types of water, 4 types of snow with different grain sizes, 16 types of soil with different textures, 15 types of mineral rocks, and 4 types of vegetation such as hay and coniferous leaves.

The spectral curves of these objects are shown in Figure 1. It shows that the numerous types of objects and the large spectral range yield a certain degree of variation, which effectively guarantees the applicability of the model. In the visible and near infrared, a largely dynamic change is seen from these spectra, where the spectral reflectance of water is low and snow is high. In the middle wave infrared and thermal infrared spectral range, the reflectance are totally low and stable.

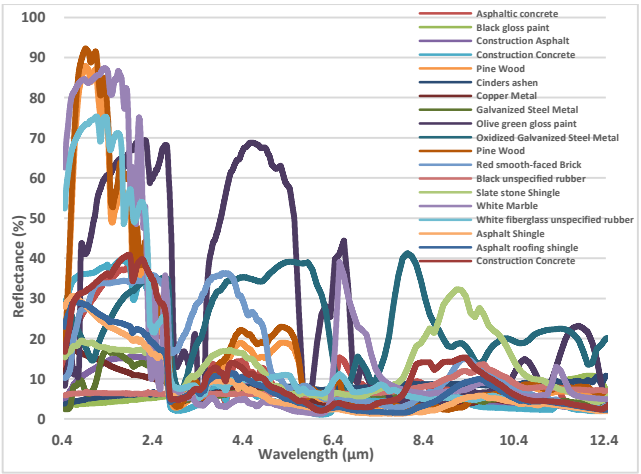

(a)manmade

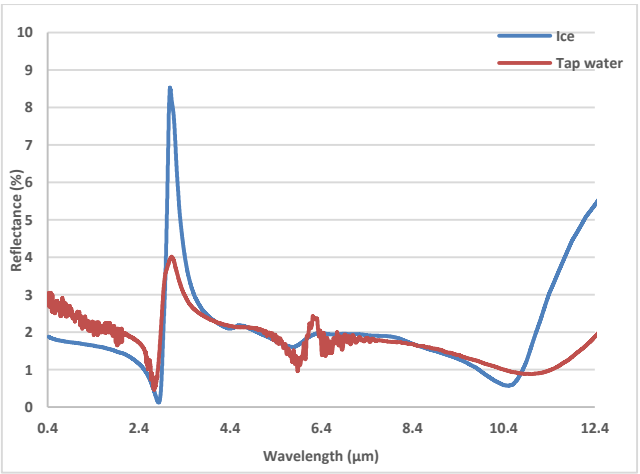

(b)water

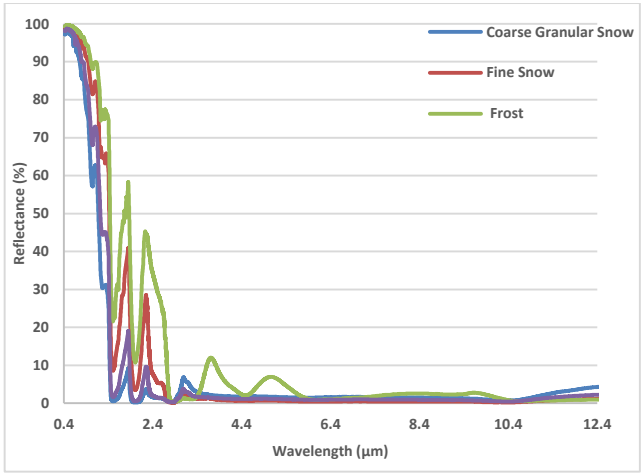

(c)snow

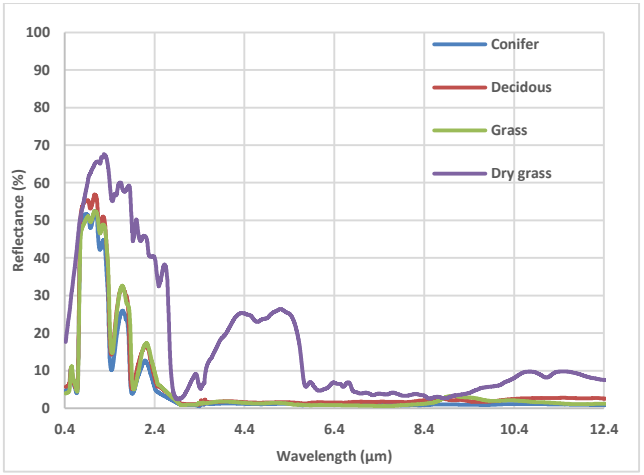

(d)vegetation

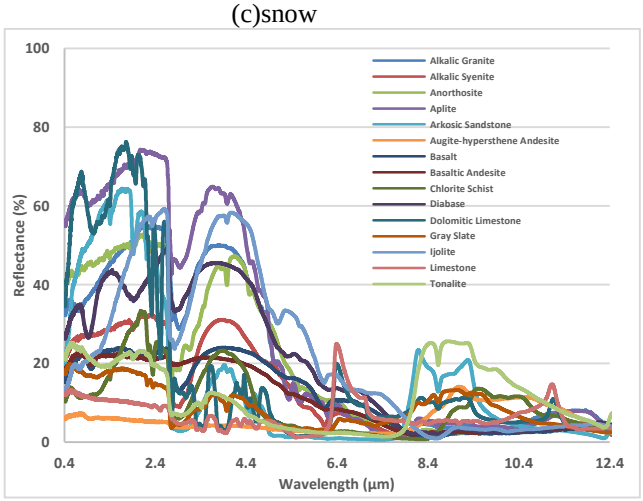

(e)rock

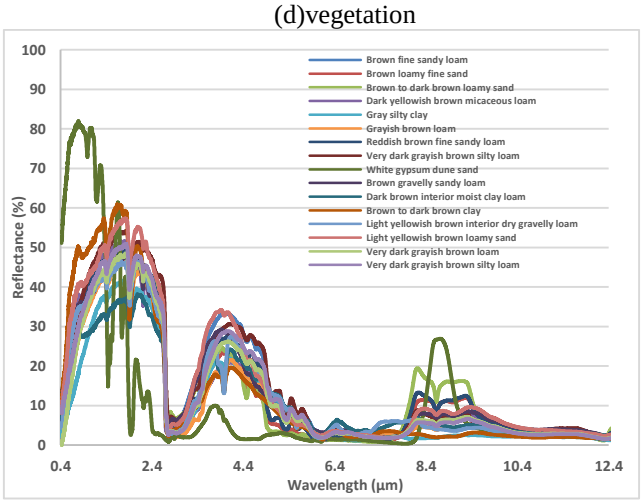

(f)soil

Figure 1. The spectral data of many types of object were selected to build the model

2.3 Spectral data equivalent calculation

In order to perform band correlation analysis and build the conversion model, the spectral data from the JHU spectral library should be equivalent calculated to match the spectral characterizes of the ASTER and VIMS sensor based on the spectral response function of each corresponding band:

$$\rho(\lambda_i) = \frac{\sum_{j=1}^{n} \rho_j(\lambda_i) f_j(\lambda_i)}{\sum_{j=1}^{n} f_j(\lambda_i)} \tag{1}$$

Where $f_j(\lambda_i)$ represents the spectral response function of the center wavelength λ_i, $\rho_j(\lambda_i)$ represents the corresponding spectral value, n represents the number of bands, and $\rho(\lambda_i)$ represents the equivalent spectral data. Based on this, the typical spectral data of 12 bands of VIMS, 14 bands of ASTER were obtained.

2.4 Data Correlation Analysis and Model

To determine which band of ASTER used for simulating the data of a certain band of VIMS, two respects are considered: 1) the band should be as close to the simulated band as possible; 2) the correlation between them should be relatively high. The coefficient r is calculated to describe the linear correlation quantitatively (Lu Jian et al., 2006):

$$\mathrm{r} = \frac{\sum (x-\bar{x})(y-\bar{y})}{\sqrt{\sum (x-\bar{x})^2 \sum (y-\bar{y})^2}} \tag{2}$$

Where x、$\bar{x}$、y and $\bar{y}$ represent their spectral data and average value of ASTER and VIMS respectively. The range of r value is -1 to 1, when r>0, it means that the two variables are positively correlated. Conversely, when r<0, it means that the two variables are negatively correlated.

The model building entails the spectral data from source channel, and its corresponding objective channel.

Based on the selected data source channel,
The image simulation model is constructed based on the selected data source channel and their spectral data. This

process uses a linear model on the basis of statistical regression analysis. There are two ways:
1) Single-band linear correlation model

$$y = ax + b \tag{3}$$

2) Multi-band linear correlation model

$$y = a_1 x_1 + ... + a_i x_i + ... + a_n x_n + b \tag{4}$$

Where y denotes the simulated band of VIMS, and x denotes the adjacent band of ASTER.

3. MODEL ANALYSIS and DATA SIMULATION

3.1 VIMS image simulation model

For the various spectra in Figure 2, their equivalent spectral values were calculated based on the spectral response functions of VIMS and ASTER bands. Then, considering the spectral distance between the bands, the coefficient r of bands are obtained. Results are shown in Table 2-6, where ASTERbi indicates the ith band of the ASTER and VIMSbi indicates the ith band of the VIMS.

Table 2. The correlation analysis between ASTER and VIMS in NIR bands

	VIMSb1	VIMSb2	VIMSb3	VIMSb4
ASTERb1	0.989	1.000	0.978	0.844
ASTERb2	0.937	0.975	1.000	0.867
ASTERb3	0.788	0.841	0.863	1.000

Table 3. The correlation analysis between ASTER band4 and VIMS band5

	VIMSb5
ASTERb4	0.996

Table 4. The correlation analysis between ASTER band5-9 and VIMS band6

	ASTER b5	ASTER b6	ASTER b7	ASTER b8	ASTER b9
VIMSb6	0.988	0.990	0.991	0.978	0.987

Table 5. The correlation analysis between ASTER SWIR-TIR bands and VIMS MIR bands

	VIMSb7	VIMSb8
ASTERb5	0.762	0.724
ASTERb6	0.763	0.733
ASTERb7	0.800	0.746
ASTERb8	0.840	0.776
ASTERb9	0.855	0.795
ASTERb10	0.215	0.227
ASTERb11	0.184	0.164
ASTERb12	0.147	0.098
ASTERb13	0.284	0.463
ASTERb14	0.354	0.548

Table 6. The correlation analysis between ASTER and VIMS in TIR bands

	VIMSb9	VIMSb10	VIMSb11	VIMSb12
ASTERb10	0.997	0.935	0.623	0.473
ASTERb11	0.945	0.998	0.613	0.411
ASTERb12	0.807	0.963	0.557	0.317
ASTERb13	0.655	0.649	0.990	0.885
ASTERb14	0.639	0.552	0.982	0.958

It can be seen from Figure 2 that the value of spectral reflectance is very low in the middle wave infrared and thermal infrared bands. The sum of reflectance and emissivity is 1 in the infrared bands based on Kirchhoff's law (Nicodemus, 1965), so the emissivity can be calculated from the reflectance data (Salisbury et al., 1994; Korb et al. (1996), and it is used to build model to improve accuracy instead of the reflectance.

For Table 2-6, a highly correlated band is selected as the data source to simulate VIMS data. The model is established based on regression analysis. Table 7 shows the selected ASTER band and its corresponding model for each band of VIMS. Where xi indicates the ith band of the ASTER data and bi indicates the ith band of the VIMS.

Table 7. Image Simulation Models for VIMS based on ASTER

VIMS (y)	ASTER (x)	R^2
b1	y=1.555x1-0.493x2-0.083x3-0.479	0.997
b2	y= x1-0.123	1
b3	y=0.998x2-0.128	1
b4	y=0.997x3-0.017	1
b5	y=0.971x4+0.762	0.992
b6	y=0.443x5+0.043x6+0.146x7+0.262x8+0.104x9+0.027	1
b7	y= -1.183x5-1.082x8+2.948x9+28.772	0.855
b8	y= -0.707x5+1.228x9-0.697x10+1.766x14-57.448	0.868
b9	y=0.891x10+0.103x14+0.758	0.997
b10	y=0.081x10+0.663x11+0.232x12+0.023x14+0.105	1.000
b11	y=0.006x10+0.569x13+0.414x14++1.079	1.000
b12	y=-0.117x11+x14+11.461	0.938

R^2 represents the coefficient of determination in Table 8. Its value is between 0-1. The closer it approaches 1, the higher the equation's goodness of fit. It is known that the value of R^2 is very high except for the middle wave infrared.

3.2 Accuracy analysis

Considering the limited spectral samples, a 10-fold-cross-validation method is used in this paper to analyze the model accuracy. Firstly, the spectral data are randomly divided into 10 parts, 9 of which are regarded as training data in rotation mode, and the remaining one is used as the actual test data. An error is yielded after each test. Finally, the error average of 10 results is taken as an estimate of the model accuracy, wherein the model in Table 7 corresponds to the case where the error is the smallest.

The simulated data of VIMS bands (denoted as y_{simu}) are calculated based on the equivalent spectral data of ASTER. The real VIMS spectral data (denoted as y_{real}) are equivalent calculated based on their spectral response functions. The relative error of y_{simu} and y_{real} is calculated to analyze the accuracy:

$$RE = \left| \frac{y_{real} - y_{simu}}{y_{simu}} \right| \tag{5}$$

The relative error of each band is shown in Table 8. The overall error in each band is small, the average error is 2.551%, most of the error is less than 1%, only the first band (blue band), 7^{th} and 8^{th} band within the middle wave infrared range. It proves that the constructed model has high accuracy and can be used for VIMS data simulation.

The simulation accuracy of these three bands is relatively low, mainly because ASTER lacks the band setting corresponding to the wavelength. The simulated band has a longer spectral distance from the source band, and the correlation is low, so the model accuracy is not very high.

Table 8. Relative Errors of the proposed model

VIMS (y)	Relative error(%)
b1	11.89
b2	0.694
b3	1.193
b4	0.711
b5	3.526
b6	0.846
b7	5.255
b8	5.285
b9	0.382
b10	0.044
b11	0.066
b12	0.723
Average	2.551

3.3 Simulated images

The VIMS data is simulated based on ASTER reflectance and emissivity product data and the established models in Table 7. The simulated area included Taihu Lake, The Jingjinji Metropolitan Region, the Daya Bay area, the Sanjiangyuan area, etc. Simulated image data of these typical areas are shared for application demonstration and Algorithm Testing. Figure 2 shows the ASTER image of the Daya Bay area at 11:08:51 on August 11, 2016; Figure 3-6 are the simulated images of VIMS in visible and near infrared, short wave infrared, middle wave infrared, and thermal infrared bands. The results show that the simulated images have rich texture characteristics, which reflects the spectral radiation differences between different materials and the difference in the same material. However, there are some strip noises in the simulated images of the thermal infrared bands. This is because the ASTER data has obvious strip noises in the thermal infrared bands (Son, 2014). It directly affected the quality of simulation results.

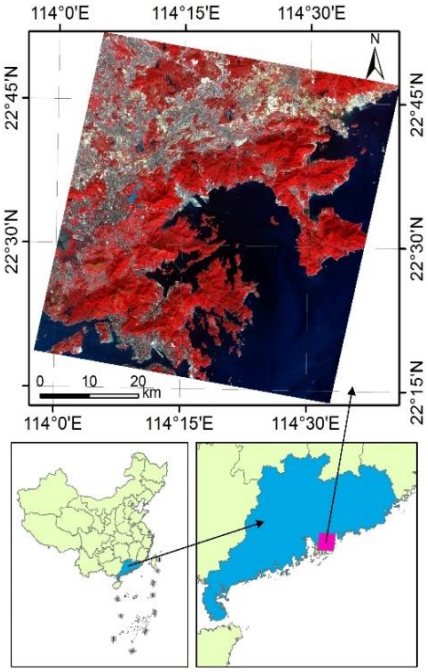

Figure 2. ASTER data for image simulation- False Color

Figure 3. VIMS Simulated image-NIR channels

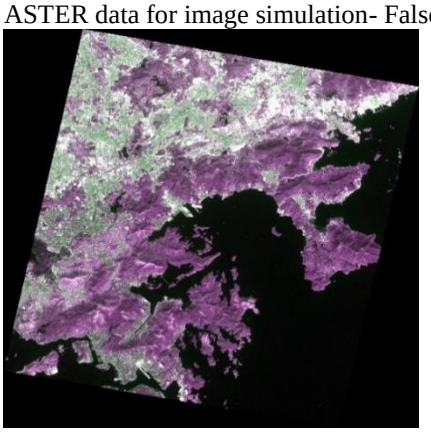

Figure 4. VIMS Simulated image-SWIR channels

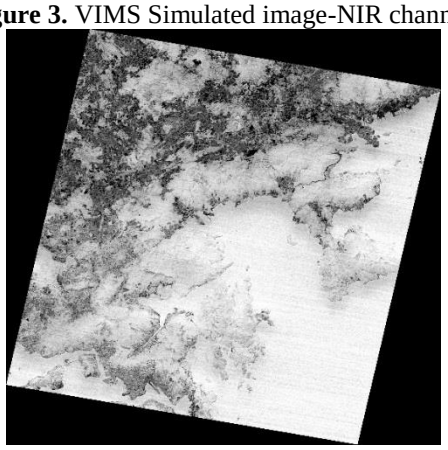

Figure 5. VIMS Simulated image-MIR channels

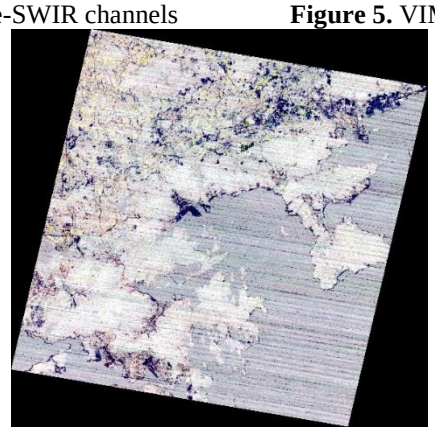

Figure 9. VIMS Simulated image-TIR channels

4. Conclusions

Remote sensing image simulation plays an important role in the development and application of new remote sensors. It provides data support in related areas: the pre-study of applied models of remote sensors, ground system construction, and its application demonstration. This paper studies the image simulation methodology of the VIMS sensor before the GF-5 satellite launch. Simulated image data of the typical areas is generated and is shared for application demonstration and Algorithm Testing.

References

[1] Baldridge A M, Hook S J, Grove C I and Rivera G. 2009. The ASTER spectral library version 2.0. Remote Sensing of Environment, 113(4): 711-715

[2] Börner A, Wiest L, Keller P, Reulke R, Richter R, Schaepman M and Schläpferb D. 2001. Sensor: a tool for the

simulation of hyperspectral remote sensing systems. ISPRS Journal of Photogrammetry and Remote Sensing, 55(5-6): 299-312.
[3] Feingersh T, Ben-Dor E and Portugali J. 2007. Construction of synthetic spectral reflectance of remotely sensed imagery for planning purposes. Environmental Modelling and Software, 22(3): 335-348
[4] Gao L R, Zhang B, Zhang X, Zhang W J and Tong Q X. 2008. A new operational method for estimating noise in hyperspectral images. IEEE Geoscience and Remote Sensing Letters, 5(1): 83-87.
[5] Korb A R, Dybwad P, Wadsworth W and Salisbury J W. 1996. Portable FTIR spectrometer for field measurements of radiance and emissivity. Applied Optics, 35(10): 1679-1692
[6] Liu Y, Zhang W J and Zhang B. 2015. Top-of-atmosphere image simulation in the 4.3-μm mid-infrared absorption bands. IEEE Transactions on Geoscience and Remote Sensing, 54(1): 452-465.
[7] Lu J, Peng M, Lu X.2006.Relativity of Remote Sensing Images and Entropy Calculation. Geomatics and Information Science of Wuhan University.31(6):476-480.
[8] Magli E. 2009. Multiband lossless compression of hyperspectral images. IEEE Transactions on Geoscience and Remote Sensing, 47(4): 1168-1178.
[9] Mobley C D and Sundman L K. 2013. Hydrolight 5.2 ecolight 5.2 users' guide. Bellevue: Sequoia Scientific, Inc, 10-22
[10] Nicodemus F E. 1965. Directional reflectance and emissivity of an opaque surface. Applied Optics, 4 (7):767-773
[11] Parente M, Clark J T, Brown A J and Bishop J L. 2010. End-to-end simulation and analytical model of remote-sensing systems: application to crism. IEEE Transactions on Geoscience and Remote Sensing, 48(11): 3877-3888.
[12] Salisbury J W, Wald A and D'Aria D M. 1994. Thermal-infrared remote sensing and Kirchhoff's law: 1. Laboratory measurements. Journal of Geophysical Research Solid Earth, 99(B6):11897-11911
[13] Segl K, Guanter L, Gascon F, Kuester T, Rogass C and Mielke C. 2015. S2etes: an end-to-end modeling tool for the simulation of sentinel-2 image products. IEEE Transactions on Geoscience and Remote Sensing, 53(10): 5560-5571.
[14] Son Y S, Kang M K and Yoon W J. 2014. Lithological and mineralogical survey of the Oyu Tolgoi region, Southeastern Gobi, Mongolia using ASTER reflectance and emissivity data. International Journal of Applied Earth Observations and Geoinformation, 26(1):205-216
[15] Sun Y Z, Jiang G W, Li Y D, Yang Y, Dai H S, He J, Wang Q, Ye J H and Cao Q. 2017. Hyper-spectral observation satellite and it's application prospects. Aerospace Shanghai, 34(3): 1-13.
[16] Tang B H, Shao K, Li Z L, Wu H and Tang R. 2015. An improved NDVI-based threshold method for estimating land surface emissivity using MODIS satellite data. International Journal of Remote Sensing, 36(19-20): 4864-4878
[17] Wang J, Zhang K and Tang S. 1995. Spectral and spatial decorrelation of Landsat-TM data for lossless compression. IEEE Transactions on Geoscience and Remote Sensing, 33(5): 1277–1285.
[18] Zhang W J. 2008. Image simulation of sagnac type imaging fourier transform spectrometer. Ph.D Dissertation, Institute of Remote Sensing Applications, Chinese Academy of Sciences.
[19] Zhao Y H, Dai L Q, Bai S J, Liu J F and Peng H G. 2017. Adance in the integrated design of visible and infrared mapping spectrometer. The 4th China High Resolution Earth Observation Conference. Wuhan.